JACS
JOURNAL OF THE AMERICAN CHEMICAL SOCIETY
Article
pubs.acs.org/JACS

Role of Water in Mukaiyama–Aldol Reaction Catalyzed by Lanthanide Lewis Acid: A Computational Study

Miho Hatanaka and Keiji Morokuma*

Fukui Institute for Fundamental Chemistry, Kyoto University, Kyoto 606-8103, Japan

Supporting Information

ABSTRACT: Carbon–carbon bond formations, such as Kobayashi modification of the Mukaiyama–Aldol reaction, catalyzed by lanthanide (Ln) Lewis acid in aqueous solution comprise one of the most attractive types of reactions in terms of green chemistry. However, their detailed mechanisms and the role of water molecules remained unclear. In order to explore complex potential energy surfaces for the water and substrate coordination around Eu^{3+} as well as the detailed mechanism of the Mukaiyama–Aldol reaction between trimethylsilyl (TMS) cylcohexenolate and benzaldehyde (BA) catalyzed by Eu^{3+}, the recently developed anharmonic downward distortion following (ADDF) and artificial force-induced reaction (AFIR) methods were used with the B3LYP-D3 theory. The most favorable water coordination structures are $Eu^{3+}(H_2O)_8$ and $Eu^{3+}(H_2O)_9$; they are comparable in free energy and are likely to coexist, with an effective coordination number of 8.3. $Eu^{3+}(H_2O)_8(BA)$ is the best aldehyde coordinated structure. Starting with this complex, the Mukaiyama–Aldol reaction proceeds via a stepwise mechanism, first C–C bond formation between the substrates, followed by proton transfer from water to BA and then TMS dissociation caused by nucleophilic attack by bulk water molecules. Why did the yield of the Mukaiyama–Aldol reaction catalyzed by Ln^{3+} in organic solvent dramatically increase upon addition of water? Without water, the reverse reaction (C–C cleavage) takes place easily. Why did this reaction show *syn*-preference in water? The *anti* transition state for C–C formation in water is entropically less favored relative to the *syn* transition state because of the existence of a rigid hydrogen bond between the TMS part and coordination water around Eu^{3+} in the former.

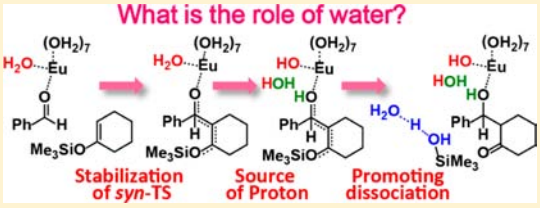

1. INTRODUCTION

Organic reactions in aqueous solution are drawing much attention as a type of green chemistry for the next generation.[1−6] Among them, carbon–carbon bond-forming reactions catalyzed by water-tolerant Lewis acids are one of the most attractive reactions.[6] Usually, Lewis acid catalysts have to be used under strictly anhydrous conditions because they are unstable and inactive in water. However, lanthanide triflates ($Ln(OTf)_3$) can catalyze many carbon–carbon or carbon–heteroatom bond-forming reactions, such as Aldol reaction, Diels–Alder reaction, Michael reaction, and Friedel–Crafts acylation.[6−12] These reactions, however, have been successful only for limited substrates, and the lack of understanding of the reaction mechanism is hindering further development. To design more efficient and highly stereoselective reactions, we need to understand the detailed reaction mechanism, especially the role of lanthanide cation and water. Several experimental studies have discussed the mechanism. Kobayashi and co-workers explored Lewis acids for the Mukaiyama–Aldol reaction in aqueous media and reported that active Lewis acids, such as lanthanide or other metal triflates and perchlorates, seemed to have a certain range of hydrolysis constants and high exchange rate constants for substitution of inner-sphere water ligands[12] as well as low nucleophilic characters.[8] These three factors must be related to the ability of substrates to coordinate to Lewis acids. However, there still are unsolved questions concerning the role of water. One question is why the product yield of the Kobayashi modification of the Mukaiyama–Aldol reaction catalyzed by $Ln(OTf)_3$ in organic solvent dramatically increased upon addition of water.[7,8] Another is why the diastereoselectivity of this aqueous reaction shows *syn*-preference. According to the experimental studies,[8,13−15] the diastereoselectivity of this reaction depends on experimental conditions, such as catalyst, solvent, additive, and pressure. For example, the same reactions under high pressure conditions[13] show *syn*-preference, while those under anhydrous conditions with Lewis acid catalyst, such as lanthanide[8] or $TiCl_4$,[14] and under hydrous conditions without catalyst[15] show *anti*-preference. To clarify the details of the reaction mechanism catalyzed by $Ln(OTf)_3$ in water, several experimental observations of intermediates of this reaction have recently been reported. Allen and co-workers measured the coordination number (CN) of water molecules around Eu^{3+} during the Mukaiyama–Aldol reaction by using luminescence decay measurements.[16,17] According to their studies, the water CN around Eu^{3+} was 8.3 in pure water solution and decreased only about 1% after aldehyde addition. A CN of about 8–9 means that almost all the OTf ligands have dissociated from Eu^{3+}.[16] The importance of the dissociative capability of ligands was also confirmed by comparison of the reaction catalyzed by $Eu(NO_3)_3$, where NO_3^- ligand is less dissociative than OTf^-.

Received: July 18, 2013
Published: August 19, 2013

   dx.doi.org/10.1021/ja407357c | J. Am. Chem. Soc. 2013, 135, 13972–13979

The water CN decreased when $Eu(NO_3)_3$ was used, resulting in a slower reaction rate.[17]

Despite a number of experimental studies, the detailed mechanism of lanthanide-catalyzed reactions in water is still unclear, and a better understanding of the mechanism is essential for development of new aqueous catalytic reactions. In the present study, we focus on the so-called Mukaiyama−Aldol reaction, shown in Scheme 1, between trimethlysilyl cylcohexenolate and benzaldehyde (BA). The reaction rate and the yield of this reaction aree greatly improved by use of a catalytic amount of $Ln(OTf)_3$.[6−8]

Scheme 1. Lanthanide Triflate-Catalyzed Mukaiyama−Aldol Reaction in Aqueous Media

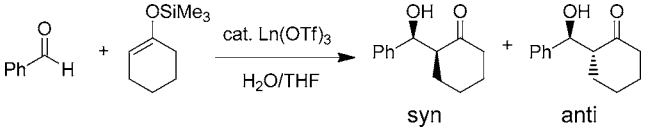

There are a few theoretical studies on the mechanism of Lewis acid-catalyzed Mukaiyama−Aldol reactions.[18−20] However, no quantum mechanical (QM) study has been reported on the mechanism with lanthanide catalyst or in water. One of the reasons for the difficulty of making QM calculations is the flexibility of the coordination geometry around a lanthanide trication (Ln^{3+}). This flexibility is related to the unique character of the electronic configuration of Ln^{3+}. The electronic configuration of Ln^{3+} is $1s^22s^22p^63s^23p^63d^{10}4s^24p^64d^{10}4f^N5s^25p^6$, where N is the number of 4f electrons. These open-shell 4f electrons are shielded by the closed-shell 5s and 5p electrons from outside. Therefore, 4f electrons usually cannot form a covalent bond with 2s and 2p electrons in organic ligands.[21] Ln^{3+} interacts with anionic ligands mainly by electrostatic and van der Waals interactions, and the coordination geometry around Ln^{3+} is independent of the direction of 4f orbitals. The ligand-to-metal charge-transfer interaction, especially with vacant 5d orbitals, does not make a large contribution, although it may make some contribution to bonding for early Ln's.[22,23] This bonding character is quite different from that of transition metals that form covalent bonds with organic ligands. In addition, the atomic radii of Ln^{3+} are larger than those of transition metals, and lanthanides have larger CNs, such as 6−12. Therefore, the structure and character of transition states (TSs) and intermediates of Ln-Lewis acid-catalyzed reactions could be different from those in the catalysis by conventional Lewis acids or by transition metal catalysts, and many reaction pathways may exist due to this flexibility of the coordination environments. A systematic and unbiased search method for a complex potential energy landscape would be needed to determine the most favorable among many possible reaction pathways.

The Global Reaction Route Mapping (GRRM) strategy developed in part in our group has been demonstrated in numerous examples to be very efficient in finding many different reaction pathways.[24] The GRRM strategy consists of two automated potential surface exploration methods. One is the anharmonic downward distortion following (ADDF) method that finds all the local minima (LMs) and TSs starting from one or a few LMs.[24−27] The other is the artificial force-induced reaction (AFIR) method that explores approximate reaction pathways starting from dissociation limits or LMs by placing an artificial force between reaction centers.[24,28,29]

In the present paper, we study the energy landscape of the entire reaction mechanism of Kobayashi modification of the Mukaiyama−Aldol reaction shown in Scheme 1, catalyzed by Eu^{3+}-Lewis acid in water,[7,8,16,17] by using the GRRM strategy. At first, in section 3.1, the optimal water CN around Eu^{3+} is determined using cluster models by application of the ADDF and AFIR methods. As already examined by both experimental[16,17,30−36] and computational[30,31,37−45] studies, a lighter Ln^{3+} predominantly has nine coordinating water molecules, whereas a heavier Ln^{3+} mainly has eight water molecules. A middle Ln^{3+}, such as Eu^{3+}, has an average water CN between 8 and 9.[16,17,30,31,33,37,44] However, the CN around Eu^{3+} in solution is still a topic of debate because the CN in water solution depends on the experimental methods, such as 8.3 by luminescence decay[16,17] and X-ray diffraction[33] and 9.0 by EXAFS.[37] In section 3.2, we also determine the most probable coordination mode of the BA substrate on Eu^{3+} in water.

In section 3.3, we study the energy landscape of the entire reaction mechanism of Mukaiyama−Aldol reaction catalyzed by Eu^{3+}-Lewis acid in water,[16,17] shown in Scheme 1, mainly by the application of the AFIR method.[24,28,29] In our previous computational study of this reaction,[46] we discussed only the diastereoselectivity of the C−C bond formation step of the reaction in Scheme 1 and demonstrated that there were many TSs whose energetic and geometric differences came from different orientations of the substrates as well as geometrical fluctuation of water molecules around Eu^{3+}. Among all the obtained TSs, 17 TSs contributed to the diastereomeric ratio, which means structural flexibility around Eu^{3+} should be essential in determining the diastereomeric ratio quantitatively. In the present study, we will simply summarize the results of the stereoselectivity of C−C bond formation step and concentrate on the other aspects of the entire Mukaiyama−Aldol reaction catalyzed by Eu^{3+}-Lewis acid in water.

2. COMPUTATIONAL DETAILS

The detailed AFIR calculation scheme is as follows. First, approximate LMs and TSs were explored by using the AFIR method. At this stage, B3LYP methods[47,48] with small basis sets, such as (7s6p5d)/[2s1p1d] on Eu^{3+} and 6-31G for others (BS0), were used. For Eu^{3+}, the Stuttgart-Dresden large-core relativistic effective core potential (RECP) was used throughout, where the 5s, 5p, 5d, 6s electrons were considered explicitly as the valence shell and six 4f electrons were put in the core potential.[49,50] This RECP has been widely used for studies of geometries of lanthanide-containing complexes, as 4f electrons are considered not to participate in bonding with ligands.[21] In all the calculations,the solvation free energy was included by the polarized continuum model (PCM)[51] with a dielectric constant of 78.3553 (water). AFIR functions were minimized with γ_{max} = 50 kcal/mol and γ_{min} = 2.5 kcal/mol; this γ_{max} value is expected to provide all reaction pathways with barriers lower than ∼50 kcal/mol. For the structure optimization of $Eu^{3+}(H_2O)_{n+1}$ in section 3.1, an artificial force was added between Eu^{3+} of optimized structures of $Eu^{3+}(H_2O)_n$ and the additional water molecule. For the optimization of the substrate-coordinated structures in section 3.2, an artificial force was added between Eu^{3+} of optimized structures of $Eu^{3+}(H_2O)_n$ and the carbonyl part of BA or the oxygen atom of trimethylsilyl (TMS) enol ether.

For the Mukaiyama−Aldol reaction,several AFIR schemes were applied in section 3.3 to explore all possible reaction pathways. To explore all possible step-by-step reaction pathways, we took every pair of fragments shown in Scheme 2 and applied forces to the pair. Note that F3 is the coordination water molecule, whereas F4 is a water molecule not in the Eu coordination shell. To explore concerted reaction pathways, artificial forces are simultaneously applied to selected three fragments, (F1, F2, F3) and (F1, F2, F4). It should be

dx.doi.org/10.1021/ja407357c | J. Am. Chem. Soc. 2013, 135, 13972−13979

Scheme 2. Fragmentation of the Reaction System for AFIR Calculation

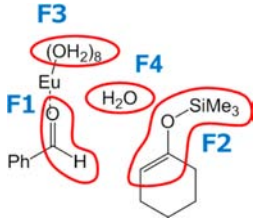

noted that,even when forces were applied to three fragments simultaneously, step-by-step reaction pathways were always obtained in the present system. In order to cover all the possible approaches, initial relative orientations of the fragments were determined randomly, and at the same time, the initial approach directions of the fragments were selected randomly. The general scheme to make random initial structures is described in ref 29.

All the approximate LM and TS geometries obtained by the initial AFIR search were reoptimized (of course without any artificial force) with the dispersion-corrected B3LYP-D3[52] with the (7s6p5d)/[5s4p3d] RECP basis set for Eu^{3+} and 6-31+G* for others (BS1). The most difficult point of the calculation of this system is the optimization of TSs, because the diagonal elements of Hessian matrixes at approximate TSs tend to have negative values not only for the reaction coordinate of target reaction but also for those of vibration and rotation of water molecules around Eu^{3+}. To solve this problem, we applied the locally updated planes (LUP) method[53,54] that enabled us to optimize the reaction pathway and the corresponding TS, using the AFIR reaction pathway as the initial guess for the LUP method. After optimization of a TS, the intrinsic reaction coordinate (IRC)[55] was calculated from the TS to two LMs to confirm the reaction pathway. After full geometry optimization, single-point calculations were performed at the B3LYP-D3[52] level with the RECP (8s7p6d)/[6s5p5d] basis set augmented with f- and g-polarization functions for Eu^{3+}[56] and cc-pVTZ for others (BS2). All these AFIR and ADDF calculations, reoptimization, and IRC calculations were performed by the GRRM program[57] using energies and energy derivatives computed by the Gaussian09 program.[58]

3. RESULTS AND DISCUSSION

3.1. Coordination Number of Water Molecules around Eu^{3+}. First, the CN of water molecules around Eu^{3+} was determined by using cluster models. Figure 1 shows the Gibbs free energies (at 298.15K, 1 atm) and the electronic energies with zero-point energy (ZPE) correction of the electronic energy-optimized structures and TSs of $Eu^{3+}(H_2O)_n$ (n = 7, 8, 9 and 10) obtained by coordination of one water molecule to an optimized coordination of $Eu^{3+}(H_2O)_{n-1}$. For instance, Cmp2 (taken as reference) is $Eu^{3+}(H_2O)_8$ with all eight water molecules directly bound to Eu^{3+} or in the first solvation shell of Eu^{3+} (plus 2 individually-PCM-immersed water molecules, for relative energy reference), while Cmp3 is $Eu^{3+}(H_2O)_8\cdots(H_2O)$, namely Cmp2 with one more second-shell water molecule coordinating two first-shell water molecules (plus one reference water molecule). As will be discussed later, there are many LM structures for each entry; in Figure 1, however, we show only the lowest energy structure for each entry. Since PCM effects are included in the calculation, if PCM is perfect in describing outer-shell coordination, Cmp2 should have the same free energy as Cmp3. In fact, based on free energy, Cmp3 is only 0.1 kcal/mol less stable than Cmp2. On the other hand, based on free energy, Cmp5 is 2.2 kcal/mol more stable than Cmp4, indicating that the PCM is not perfect, and the agreement between Cmp3 and Cmp2 is a little fortuitous.

A more reasonable comparison should be between Cmp4 and Cmp3. This is the energy required to move one water molecule from the second shell to the first shell that involves direct contact with the Eu^{3+}. This energy difference is 0.6 kcal/mol, indicating that these two structures can coexist at 298.15 K, 1 atm. On the other hand, Cmp6 is 8.3 kcal/mol higher in free energy than Cmp5, indicating that Cmp6 with 10 H_2O molecules in the first shell is substantially less stable than Cmp5 with 9 H_2O's in the first shell. Thus the thermodynamic contribution of Cmp6 can be completely neglected. Similarly, Cmp1 with only 7 H_2O's in the first shell is 4.7 kcal/mol less stable than Cmp2. Thus the thermodynamic contribution of Cmp1 can also be completely neglected. Therefore the dominant hydration species in solution should be $Eu^{3+}(H_2O)_8$ and $Eu^{3+}(H_2O)_9$. The average water CN in the first solvation shell can be estimated to be thermodynamic average between Cmp2 and Cmp4, and is calculated to be 8.3. Experimental CN is 8.3 by luminescence-decay method[16,17] and X-ray diffraction,[33] and theoretical CN by molecular dynamics simulation is 8.4.[44] The present results agree nearly quantitatively with these estimates. Although complex with CN = 9 was suggested by several other studies,[37−39,42,43] no previous studies suggested $Eu^{3+}(H_2O)_7$ or $Eu^{3+}(H_2O)_{10}$, all consistent with the present results.

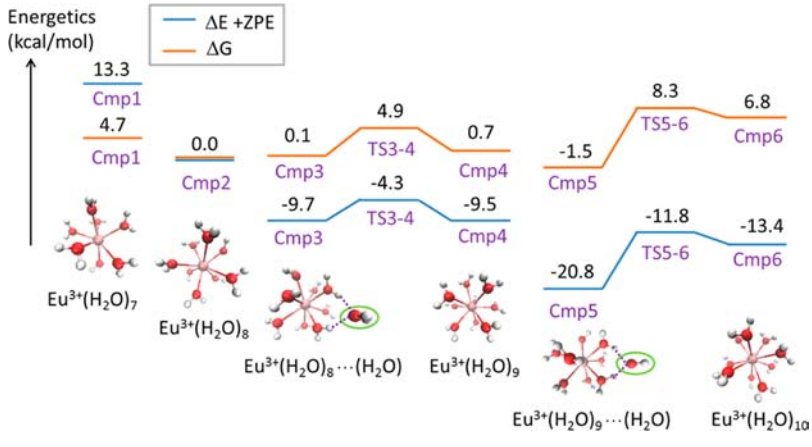

Figure 1. Energy profiles (the Gibbs free energies in orange and electronic energies with zero-point energy correction in blue, in kcal/mol) of one-water coordination to n-water-coordinated Eu^{3+} (n = 7, 8, 9). The reference energy is Cmp2 + two individually-PCM-immersed water molecules.

dx.doi.org/10.1021/ja407357c | J. Am. Chem. Soc. 2013, 135, 13972−13979

In the above discussion we used the Gibbs free energy calculated with full entropic contribution for the coordination process: $Eu^{3+}(H_2O)_n + H_2O \rightarrow Eu^{3+}(H_2O)_{n+1}$. However, in the present situation, one H_2O molecule is moved from a solvent bulk, not from the gas phase, to the coordination state. Thus some of the gas phase "entropy" must be quenched in bulk solvent. Thus for a comparison, in Figure 1, we also give values of the electronic energy (ΔE) + ZPE correction that contains no entropy. Although there have been various proposals concerning the entropy contributions in such a situation,[59−72] we simply say here that the true value is between ΔG and ΔE + ZPE, somewhat closer to ΔG. In the present situation shown in Figure 1, the difference between $Eu^{3+}(H_2O)_8$ and $Eu^{3+}(H_2O)_9$ did not change much between the two energy scales, $Eu^{3+}(H_2O)_7$ can be completely neglected, and $Eu^{3+}(H_2O)_{10}$, Cmp6, is also neglected compared to Cmp5, even if the entropy is completely ignored. Thus the overall qualitative conclusions did not depend on the level of quenching of entropic contribution.

The coordination of a water molecule to the seven-water-coordinated $Eu^{3+}(H_2O)_7$ (Cmp1) proceeds without reaction barrier to reach $Eu^{3+}(H_2O)_8$ (Cmp2). Namely, the added water molecule never gets trapped as an external water like $Eu^{3+}(H_2O)_7\cdots(H_2O)$. One can say that $Eu^{3+}(H_2O)_7$ has enough space to accommodate another water molecule in the first shell. On the other hand, there is a substantial barrier at TS3_4 between $Eu^{3+}(H_2O)_8\cdots(H_2O)$ (Cmp3) and $Eu^{3+}(H_2O)_9$ (Cmp4). The barrier from the reactant (Cmp3) to the TS (TS3_4) is 4.8 kcal/mol for the Gibbs free energy and 5.4 kcal/mol for the electronic energy with ZPE correction. The origin of TS3_4 is the distortion of the first shell solvation structure as well as the loss of hydrogen bond stabilization of the external water molecule (in green circle in Figure 1). For the external water molecule in Cmp3 to come into the first solvation shell, a space has to be created in the $Eu^{3+}(H_2O)_8$ first shell by distorting water-Eu-water angles requiring the distortion energy and at the same time the external water molecule has to break one of the two hydrogen bonds it had in Cmp3 losing the interaction energy, before it can come into the first solvation shell and interact strongly with the Eu^{3+}, as seen clearly in Figure S1 (Supporting Information).

As mentioned in Introduction, the geometry around Eu^{3+} fluctuates because of the ionic and nondirectional character of bonds between Eu^{3+} and ligands. Therefore, there may be a number of LMs whose geometries are slightly different. To find other geometries of eight- and nine-water-coordinated Eu^{3+}, a systematic search of LMs using the ADDF calculation was carried out. For eight-water-coordinated Eu^{3+}, 22 LMs are found and can be roughly categorized into two groups. One has the so-called square antiprism (SA) structure and the other has the distorted square antiprism (DSA) or bicapped trigonal prism (BTP) structure as shown in Figure 2. The most stable SA structure is 3.9 kcal/mol more stable than that of the DSA structure. There are also LMs whose geometries are the mixture of SA and DSA and relative Gibbs free energies are distributed from 0.1 through 4.6 kcal/mol. For nine-water-coordinated Eu^{3+}, 24 LMs are found whose structures are so-called the tricapped trigonal prism (TTP) or the monocapped square antiprism (MSA) as shown in Figure 2. Most LMs have the TTP structures, while some of them have the distorted structures. Their energies are distributed from 0.0 to 5.9 kcal/mol. The average bond length between Eu^{3+} and O atoms are 2.48, 2.51, and 2.50 Å for SA, DSA(or BTP), and TTP

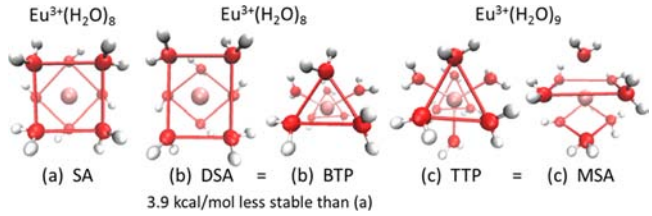

Figure 2. Geometries of eight-water-coordinated Eu^{3+}: the square antiprism (SA) structure (a) and the distorted square antiprism (DSA) or bicapped trigonal prism (BTP) structure (b). Geometry of nine-water-coordinated Eu^{3+}: the tricapped trigonal prism (TTP) structure or the monocapped square antiprism (MSA) structure (c).

structures, respectively. Compared with experimental studies, they are good agreement with the recent EXAFS data of 2.47 ± 0.007 Å,[37] and X-ray diffraction data of 2.450 Å.[33] Note that compounds shown in Figure 1 have SA structures for Cmps 2 and 3 and TTP structures for Cmps 4 and 5. Therefore, even if the structural fluctuation around Eu^{3+} is considered, the energetics of Eu^{3+} with different CN of water shown in Figure 1 does not change so much.

3.2. Coordination between $Eu^{3+}(H_2O)_n$ and Benzaldehyde. The energetics of coordination of a substrate is considered next. In this system, there are two substrates, BA and TMS enol ether. However, it has been found that TMS enol ether cannot coordinate directly to Eu^{3+} stably and tends to move out into the second coordination shell. This is probably because the latter structure is stabilized by hydrogen bonds between hydrogen in coordination water and oxygen in the enol part.

Therefore, only the structures and energetics of BA coordination are calculated, as show in Figure 3. Cmp7 is the $Eu^{3+}(H_2O)_8\cdots(BA)$, where BA is coordinated in the second solvation shell, via hydrogen bonding to two of the first shell water molecules. Cmp8 is $Eu^{3+}(H_2O)_8(BA)$, with BA in the first solvation shell, resulting in the total coordination number of CN = 9. Cmp8 is more stable in free energy than Cmp7 by 1.7 kcal/mol, suggesting that the Cmp8 will be more dominant than Cmp7. There exist a free-energy barrier of 4.6 kcal/mol for going from Cmp7 to Cmp8, or the energy required to move BA from the second shell to the first shell without changing water coordination mode; this reaction step should proceed smoothly at room temperature. There are two geometries for $Eu^{3+}(H_2O)_8(BA)$, because the nine coordination points in the TTP structure are not equivalent. Although another type of TTP structure (see Figure S2) has a lower reaction barrier, Cmp8 is the most stable geometry for $Eu^{3+}(H_2O)_8(BA)$.

From Cmp9, $Eu^{3+}(H_2O)_9\cdots(BA)$ with CN = 9, there is an intermediate Cmp10, $Eu^{3+}(H_2O)_9(BA)$ with 10 ligands in the first shell (CN = 10), and then another intermediate Cmp11, $Eu^{3+}(H_2O)_8(BA)\cdots(H_2O)$ with CN = 9. The free energy indicates clearly that Cmp11, with one water molecule that moved out of the first solvation shell, is thermodynamically the most stable of these three species. Therefore, we can say that the most populated BA-coordinated complex is Eu^{3+} coordinated by eight water molecules and a BA (Cmp8 and Cmp11). It is also consistent with the experimental CN of water (8.2), slightly smaller than that before addition of BA.[16,17] Therefore, we will discuss the mechanism of Mukaiyama−Aldol reaction by using Cmp8 in the following section.

3.3. Mechanism of Aqueous Mukaiyama−Aldol Reaction Catalyzed by Eu^{3+}. *Search for Concerted Pathways.*

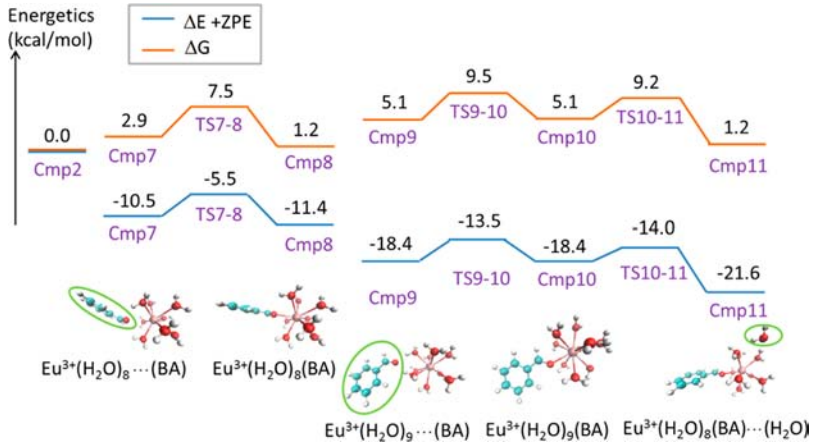

Figure 3. Energy profiles (the Gibbs free energies in orange and electronic energies with zero-point energy correction in blue, in kcal/mol) for coordination of benzaldehyde (BA) to *n*-water-coordinated Eu^{3+} (n = 8, 9). The reference energy is that of a Cmp2 + PCM-immersed BA molecule.

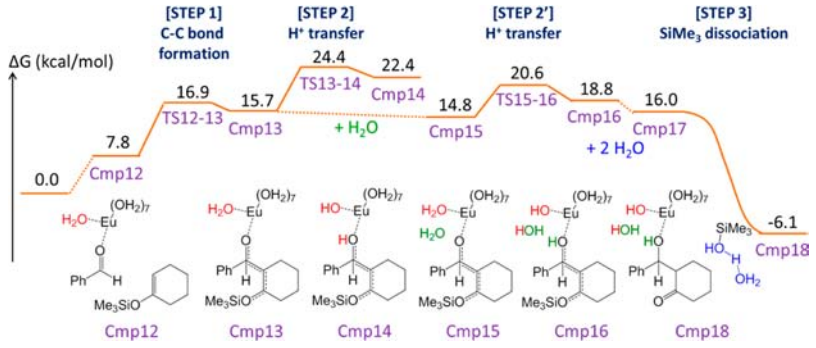

Figure 4. Gibbs free energy profile (in kcal/mol) of aqueous Mukaiyama–Aldol reaction catalyzed by $Eu^{3+}(H_2O)_8$. Compounds with the same number of atoms are connected with solid lines. Dot lines are used to connect compounds with different number of atoms. The reference of the energy (ΔG = 0.0 kcal/mol) is Cmp8 ($Eu^{3+}(H_2O)_8(BA)$) + TMS enol ether.

Based on the structure and energetics obtained in the previous two subsections, we take Cmp12, $Eu^{3+}(H_2O)_8(BA)\cdots(EE)$, the optimized structure of the complex of $Eu^{3+}(H_2O)_8(BA)$ (Cmp8) with one EE (EE = TMS enol ether) molecule in the second solvation shell, as the starting point of the reaction. From this starting point we searched possible reaction pathways for the Mukaiyama–Aldol reaction by using the AFIR systematic reaction path search calculations. This reaction should consist of three reaction elements: C–C bond formation, proton transfer, and TMS dissociation. We do not know in which order these three elements take place nor whether these elements proceed stepwise or concertedly. Therefore, in order to take into count all the possibilities, AFIR search was made for all reactions between all combinations of fragments shown in Scheme 2. First, artificial forces are places simultaneously between all pairs of BA (F1), TMS enol ether (F2), and water (F3 or F4), in order to explore concerted reaction pathways. Although initial AFIR search gave some approximate pathways for concerted reactions, reoptimization without artificial forces converted all of them to stepwise reaction pathways. (For details, see Figure S3.) Therefore, we conclude that concerted pathways do not exist within ~50 kcal/mol from the isolated fragments.

C–C Bond Formation. The most favorable reaction pathway thus obtained is shown in Figure 4, for that producing the *syn*-structure. That for the *anti*-structure is qualitatively similar.[46] This reaction starts with the C–C bond formation (step 1), followed by proton transfer from coordinated or bulk water molecules to BA (step 2) and then TMS dissociation caused by nucleophilic attack by bulk water molecules (step 3). As discussed in our previous study,[46] the reaction barrier of C–C bond formation depends on the orientation between two substrates and the fluctuating structure around Eu^{3+}. The orientation between two substrates is determined by the $(OSiMe_3)C-C-C-O$ dihedral angle ϕ defined in Figure 5. As was discussed in detail in ref 46, the dihedral angles ϕ of Cmp12, TS12-13, and Cmp13 are all around 180° where the barrier is the lowest.

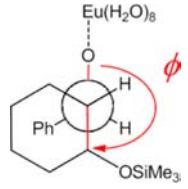

Figure 5. Definition of the dihedral angle ϕ.

Proton Transfer from Water to Aldehyde. The barrier of the next step from Cmp13, proton transfer from water to aldehyde, is a little complicated because it depends on the number of water molecules that mediate the proton transfer. As shown in Figure 4, the reaction barrier at TS13-14 for the direct proton transfer from the nearest first-shell water to BA is 8.7 kcal/mol, relative to Cmp13. However, the same reaction mediated by a water molecule in the second solvation shell has

dx.doi.org/10.1021/ja407357c | J. Am. Chem. Soc. 2013, 135, 13972–13979

a lower barrier of 5.8 kcal/mol (TS15-16). In the real water solution, this barrier may have a lower value because many water molecules connected by an extended hydrogen-bond network may mediate this proton transfer. In any case, the reaction barrier measured from Cmp12 is at most 16.6 kcal/mol (TS13-14), which is reasonable value for a reaction at room temperature.

TMS Dissociation. In the final step, the TMS group is dissociated by nucleophilic attack of water molecules. It is also difficult to say how many water molecules mediate this step. However, the present calculations show that two bulk water molecules can promote this step (Cmp17 to Cmp18 in Figure 2), and the dissociation of TMS group proceeds without barrier. In this step, one of the bulk water molecules has an OH^- character because of the partial proton transfer to another water, and the water with OH^- character attacks the TMS group nucleophilically. Note that when the dihedral angle ϕ is about −60° (in contrast to −180° in Figure 2), the TMS group is close to Eu^{3+} and the OH^- group from the coordinating water on Eu^{3+} may directly make a nucleophilic attack at the TMS group (as is seen for P3−P5 in Figure S3). However, this barrier of the TMS dissociation is 19.0 kcal/mol, and the total overall reaction barrier measured from Cmp12 becomes 36.8 kcal/mol, too large in the room-temperature condition. Therefore, it can be said that what promotes TMS dissociation is not coordinating water but bulk water molecules.

Reactions Starting with Proton Transfer or TMS Dissociation. We also explored other possibilities that the reaction starts from proton transfer or TMS dissociation. First, to explore possible reaction pathways starting from proton transfer from water to BA, the AFIR force was added between BA (F1) and coordination water (F3) or bulk water (F4). However, no reaction pathways whose barriers are less than 50 kcal/mol are obtained. Second, the AFIR force was added between TMS enol ether and water to explore possible reaction pathways starting from TMS dissociation. Two reaction pathways producing corresponding enol and ketone are obtained (see Figure S4). However, their reaction barriers are more than 40 kcal/mol, which are too large at room temperature. The same reaction between TMS enol ether and coordination water around Eu^{3+} (F3) does not proceed because the O atom in a water does not face TMS and cannot initiate the nucleophilic attack. Therefore, we conclude that reactions starting from proton transfer or TMS dissociation are unfavorable compared with those starting from C−C bond formation.

Role of Water Molecules in the Yield and Diastereoselectivity. Finally, we answer two critical questions raised in Introduction concerning the role of water molecules in this reaction. The first question is *why the yield of this reaction in organic solvent increases dramatically upon addition of water.*[7,8] Although we have not performed explicit calculations for organic solvent, an answer may be found by the nature of the Gibbs free energy surface of the reaction in Figure 4. The intermediate (Cmp13) formed after C−C bond formation is less stable than the reactant (Cmp12), and the backward reaction barrier from Cmp13 to TS12_13 is only 1.2 kcal/mol. Therefore, the backward reaction seems to proceed more easily than the forward reaction. In water solvent, however, the equilibrium would shift to the forward direction because the product is well stabilized after TMS dissociation (Cmp18). Therefore, the forward reaction from Cmp12 to Cmp18 is promoted. On the other hand, in organic solvent neither proton source nor nucleophile, such as extra water molecule, exists in the system, so that we can guess that both proton transfer and TMS dissociation should not proceed. Therefore, in the absence of water, the backward reaction from Cmp13 to Cmp12 should proceed easily, slowing down the overall reaction.

The second question, *why this reaction shows syn-preference*,[8] can be understood by comparing two lowest TSs for C−C bond formation producing *syn*- and *anti*-structures. Because C−C bond formation step is the diastereo-determining step, diastereoselectivity is determined by the energy difference between the TSs producing *syn* and *anti* structures. As discussed previously,[46] there are 17 lower TSs that contribute to the quantitative diastereomeric ratio. However, qualitatively we can focus only on the lowest TS that produces the -structure and the lowest TS that produces the *anti*-structure. The lowest *syn*-TS, with $\phi \approx 180°$ is more stable in free energy than the lowest *anti*-TS with $\phi \approx 53°$ by 0.40 kcal/mol (see Figure 6).

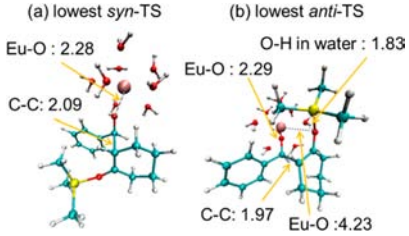

Figure 6. Geometries of the lowest TS (TS12-13) producing *syn*- (a) and *anti*-products (b).

Comparing the two structures, in the *anti*-TS the phenyl group, the cyclohexene group and the TMS group do not face each other (Figure 6) and have less steric repulsion. In fact, the electronic energy and the energy with ZPE correction of the lowest *anti*-TS are more stable than the lowest *syn*-TS by 1.1 and 0.43 kcal/mol, respectively. However, the entropy stabilization $-T\Delta S$ for the lowest *syn*-TS is larger, making the *syn*-TS more stable in Gibbs free energy than the lowest *anti*-TS. The lowest *anti*-TS is less flexible because the oxygen atom of enol ether part is fixed by the hydrogen bond between with a hydrogen of a coordination water.[46] Therefore, we can say that the lowest *anti*-TS is "destabilized entropically" by coordination water molecules and becomes less stable in free energy than the lowest *syn*-TS. It might be one of the reasons why the diastereoselectivity of this reaction depends on the experimental conditions. We can propose a possible reason why the diastereoselectivity of this reaction changes from *anti*-preference to *syn*-preference by addition of water, though we did not calculate the TSs of C−C bond formation under anhydrous condition. The lowest *anti*-TS which has the smallest steric repulsion should be most stable under anhydrous condition because of the lack of entropic destabilization effect caused by coordination water.

As shown above, there are many factors that control stereoselectivity, such as steric repulsion, stabilization by hydrogen bond, destabilization by entropic effect, and so on. In the present system, the steric repulsion between the current substrates is not very dominant and the diastereoselectivity depends heavily on the experimental conditions, such as metal in catalyst, pressure, additive, and solvent.[8,13−15] One may think that lanthanide is not suitable to achieve high stereoselectivity because of the structural fluctuation around lanthanide as

dx.doi.org/10.1021/ja407357c | J. Am. Chem. Soc. 2013, 135, 13972−13979

shown in our previous study.[46] However, there are many reports that achieve high stereoselectivity using lanthanide and chiral ligands.[73−80] How these reaction systems control the stereoselectivity by using lanthanide cations whose coordination geometry fluctuate should be an interesting future subject.

4. CONCLUSIONS

This paper describes a detailed investigation of mechanism of aqueous Mukaiyama−Aldol reaction catalyzed by Eu^{3+} and answers questions about the role of water molecules. First, the geometry and coordination number of water around Eu^{3+} in the first solvation shell in aqueous media is discussed by using cluster models. To discuss their stability, we compare the energetics of reactants, products, and transition states of a water coordination reaction to *N*-water-coordinated Eu^{3+}, where N = 7−9, and clarify that eight- and nine-water-coordinated Eu^{3+} can coexist at room temperature which is consistent with the experimental CN.[16,17,33] The most stable structures of eight- and nine-water coordinated Eu^{3+} have the square antiprism and tricapped trigonal prism structures, respectively. Second, BA coordination to Eu^{3+} surrounded by several water molecules is also examined. Coordination of BA to eight- and nine-water-coordinated Eu^{3+} proceeds easily, although coordination of a BA to Eu^{3+} coordinated already by nine water molecules proceeds with dissociation of one coordinated water molecule to the second solvation shell. Therefore, the most stable complex, Eu^{3+} coordinated with eight water molecules and a BA, is used as a reactant of aqueous Mukaiyama−Aldol reaction.

The mechanism of aqueous Mukaiyama−Aldol reaction catalyzed by Eu^{3+} is examined by the AFIR method. The most favorable reaction pathway is the stepwise reaction starting from C−C bond formation followed by proton transfer from water to BA and then TMS dissociation caused by nucleophilic attack of a bulk water molecule. We would like to emphasize that exploring without prejudice the reaction pathways for systems with large number of atoms, components, reaction steps, and fluctuating geometries is now doable by using AFIR method.

Two questions about the role of water for this reaction are answered. One question, why the yield of Mukaiyama−Aldol reaction catalyzed by Ln^{3+} is highly improved by addition of water, can be answered on the basis of the nature of the Gibbs free energy surface along the reaction pathway. Without water, the proton transfer and TMS dissociation cannot proceed smoothly. The backward reaction proceeds with lower barrier than the forward reaction under anhydrous condition, which results in the low yield of the product. With water, proton transfer takes place smoothly and the dissociation of TMS takes place without barrier, improving the yield of the overall reaction. The other question why this aqueous reaction shows *syn* preference is explained by entropic effect on the TSs of C−C bond formation step. Although the lowest *anti*-TS has the lower potential energy than the lowest *syn*-TS because of the smaller steric repulsion, the entropic effect makes for the lowest *anti*-TS is less favorable than for the lowest *syn*-TS, because the lowest *anti*-TS has less structural flexibility caused by hydrogen bond between TMS enol ether and coordination water. This results in the higher Gibbs free energy of the *anti*-TS than that of the *syn*-TS. As shown above, the roles of water for this reaction are to stabilize the product by promoting TMS dissociation by nucleophilic attack, and to supply a proton to aldehyde. The demerit of this reaction is low diastereoselectivity mainly caused by structural fluctuation of coordination water around Eu^{3+} in the diastereo-determining TS. A better way to restrict fluctuation of coordinating water structures by appropriate ligands is needed to improve the diastereoselectivity of the Ln-catalyzed reaction.

■ ASSOCIATED CONTENT

Supporting Information

Detailed scheme of AFIR calculation, energy profiles of minor reaction pathways, and Cartesian coordinates of all the intermediates and transition states. This material is available free of charge via the Internet at http://pubs.acs.org.

■ AUTHOR INFORMATION

Corresponding Author

morokuma@fukui.kyoto-u.ac.jp

Notes

The authors declare no competing financial interest.

■ ACKNOWLEDGMENTS

We are grateful to Prof. Satoshi Maeda of Hokkaido University for helpful discussions about ADDF and AFIR methods. This work was supported in part by a CREST (Core Research for Evolutional Science and Technology) grant in the Area of High Performance Computing for Multiscale and Multiphysics Phenomena from the Japanese Science and Technology Agency (JST) and in part by grants from Japan Society for the Promotion of Science (Grants-in-Aid for Scientific Research <KAKENHI> No. 24245005 and 25109525) at Kyoto University. M.H. acknowledges the Fukui Fellowship of Kyoto University. The computer resources at the Academic Center for Computing and Media Studies (ACCMS) at Kyoto University and Research Center of Computer Science (RCCS) at the Institute for Molecular Science are also acknowledged.

■ REFERENCES

(1) Li, C.-J. *Green Chem.* **2008**, *10*, 151−152.
(2) Jung, Y.; Marcus, R. A. *J. Am. Chem. Soc.* **2007**, *129*, 5492−5502.
(3) Mase, N.; Nakai, Y.; Ohara, N.; Yoda, H.; Takabe, K.; Tanaka, F.; Barbas, C. F., III *J. Am. Chem. Soc.* **2006**, *128*, 734−735.
(4) Li, C.-J. *Chem. Rev.* **2005**, *105*, 3095−3166.
(5) Blake, J. F.; Jorgensen, W. L. *J. Am. Chem. Soc.* **1991**, *113*, 7430−7432.
(6) Kobayashi, S.; Sugiura, M.; Kitagawa, H.; Lam, W. W. L. *Chem. Rev.* **2002**, *102*, 2227−2302.
(7) Kobayashi, S. *Synlett* **1994**, 689−701.
(8) Kobayashi, S.; Hachiya, I. *J. Org. Chem.* **1994**, *59*, 3590−3596.
(9) Kawada, A.; Mitamura, S.; Kobayashi, S. *J. Chem. Soc., Chem. Commun.* **1993**, 1157−1158.
(10) Kobayashi, S.; Hachiya, I. *Tetrahedron Lett.* **1992**, *33*, 1625−1628.
(11) Kobayashi, S. *Chem. Lett.* **1991**, 2187−2190.
(12) Kobayashi, S.; Nagayama, S.; Busujima, T. *J. Am. Chem. Soc.* **1998**, *120*, 8287−8288.
(13) Yamamoto, Y.; Maruyama, K. *J. Am. Chem. Soc.* **1983**, *105*, 6963−6965.
(14) Mukaiyama, T.; Banno, K.; Narasaka, K. *J. Am. Chem. Soc.* **1974**, *96*, 7503−7509.
(15) Lubineau, A.; Meyer, E. *Tetrahedron* **1988**, *44*, 6065−6070.
(16) Dissanayake, P.; Allen, M. J. *J. Am. Chem. Soc.* **2009**, *131*, 6342−6343.
(17) Averill, D. J.; Dissanayake, P.; Allen, M. J. *Molecules* **2012**, *17*, 2073−2081.
(18) Lee, J. M.; Helquist, P.; Wiest, O. *J. Am. Chem. Soc.* **2012**, *134*, 14973−14981.

(19) Wong, C. T.; Wong, M. W. *J. Org. Chem.* **2007**, *72*, 1425−1430.
(20) Wang, L.; Wong, M. W. *Tetrahedron Lett.* **2008**, *49*, 3916−3920.
(21) Maron, L.; Eisenstein, O. *J. Phys. Chem. A* **2000**, *104*, 7140−7143.
(22) Clark, D. L.; Gordon, J. C.; Hay, P. J.; Poli, R. *Organometallics* **2005**, *24*, 5747−5758.
(23) Krogh-Jespersen, K.; Romanelli, M. D.; Melman, J. H.; Emge, T. J.; Brennan, J. G. *Inorg. Chem.* **2010**, *49*, 552−560.
(24) Maeda, S.; Ohno, K.; Morokuma, K. *Phys. Chem. Chem. Phys.* **2013**, *15*, 3683−3701.
(25) Ohno, K.; Maeda, S. *Chem. Phys. Lett.* **2004**, *384*, 277−282.
(26) Maeda, S.; Ohno, K. *J. Phys. Chem. A* **2005**, *109*, 5742−5753.
(27) Ohno, K.; Maeda, S. *J. Phys. Chem. A* **2006**, *110*, 8933−8941.
(28) Maeda, S.; Morokuma, K. *J. Chem. Phys.* **2010**, *132*, 241102−241106.
(29) Maeda, S.; Morokuma, K. *J. Chem. Theory Comput.* **2011**, *7*, 2335−2345.
(30) Helm, L.; Merbach, A. E. *Chem. Rev.* **2005**, *105*, 1923−1959.
(31) Helm, L.; Merbach, A. E. *Coord. Chem. Rev.* **1999**, *187*, 151−181.
(32) Marcus, Y. *Chem. Rev.* **1988**, *88*, 1475−1498.
(33) Habenschuss, A.; Spedding, F. H. *J. Chem. Phys.* **1980**, *73*, 442−450.
(34) Crossy, C.; Helm, L.; Powell, D. H.; Merbach, A. E. *New J. Chem.* **1995**, *19*, 27−35.
(35) Allen, P.; Bucher, J. J.; Shuh, D. K.; Edelstein, N. M.; Craig, I. *Inorg. Chem.* **2000**, *39*, 595−601.
(36) Ishiguro, S.-I.; Umebayashi, Y.; Kato, K.; Takahashi, R.; Ozutsumi, K. *J. Chem. Soc., Faraday Trans.* **1998**, *94*, 3607−3612.
(37) Duvail, M.; Zitolo, A.; Migliorati, V.; Chillemi, G.; Duvail, M.; Vitorge, P.; Abadie, S.; Spezia, R. *Inorg. Chem.* **2011**, *50*, 4572−4579.
(38) Duvail, M.; Vitorge, P.; Spezia, R. *Chem. Phys. Lett.* **2010**, *498*, 90−96.
(39) Duvail, M.; Vitorge, P.; Spezia, R. J. *Chem. Phys.* **2009**, *130*, 104501−104512.
(40) Beuchat, C.; Hagberg, D.; Spezia, R.; Gagliardi, L. *J. Phys. Chem. B* **2010**, *114*, 15590−15597.
(41) Fujiwara, T.; Mori, H.; Mochizuki, Y.; Tatewaki, H.; Miyoshi, E. *J. Mol. Struct.: THEOCHEM* **2010**, *949*, 28−35.
(42) Duvail, M.; Spezia, R.; Vitorge, P. *ChemPhysChem* **2008**, *9*, 693−696.
(43) Duvail, M.; Souaille, M.; Spezia, R.; Cartailler, T.; Vitorge, P. *J. Chem. Phys.* **2007**, *127*, 034503−034513.
(44) Clavaguéra, C.; Pollet, R.; Soudan, J. M.; Brenner, V.; Dognon, J. P. *J. Phys. Chem. B* **2005**, *109*, 7614−7616.
(45) Cosentino, U.; Villa, A.; Pitea, D.; Moro, G.; Barone, V. *J. Phys. Chem. B* **2000**, *104*, 8001−8007.
(46) Hatanaka, M.; Maeda, S.; Morokuma, K. *J. Chem. Theory Comput.* **2013**, *9*, 2882−2886.
(47) Lee, C. T.; Yang, W. T.; Parr, R. G. *Phys. Rev. B* **1988**, *37*, 785−789.
(48) Becke, A. D. *J. Chem. Phys.* **1993**, *98*, 5648−5652.
(49) Dolg, M.; Stoll, H.; Savin, A.; Preuss, H. *Theor. Chim. Acta* **1989**, *75*, 173−194.
(50) Dolg, M.; Stoll, H.; Preuss, H. *Theor. Chim. Acta* **1993**, *85*, 441−450.
(51) Tomasi, J.; Mennucci, B.; Cammi, R. *Chem. Rev.* **2005**, *105*, 2999−3093.
(52) Grimme, S.; Antony, J.; Ehrlich, S.; Krieg, H. *J. Chem. Phys.* **2010**, *132*, 154104−154119.
(53) Ulitsky, A.; Elber, R. *J. Chem. Phys.* **1990**, *92*, 1510−1511.
(54) Choi, C.; Elber, R. *J. Chem. Phys.* **1991**, *94*, 751−760.
(55) Fukui, K. *Acc. Chem. Res.* **1981**, *14*, 363−368.
(56) Yang, J.; Dolg, M. *Theor. Chem. Acc.* **2005**, *113*, 212−224.
(57) Maeda, S.; Osada, Y.; Morokuma, K.; Ohno, K. *GRRM*, a developmental version at Kyoto University.
(58) Frisch, M. J.; et al.. *Gaussian 09*, revision D.01; Gaussian, Inc.: Wallingford, CT, 2009.
(59) Tanaka, R.; Yamashita, M.; Chung, L. W.; Morokuma, K.; Nozaki, K. *Organometallics* **2011**, *30*, 6742−6750.
(60) Ribeiro, R. F.; Marenich, A. V.; Cramer, C. J.; Truhlar, D. G. *J. Phys. Chem. B* **2011**, *115*, 14556−14562.
(61) Ho, J.; Klamt, A.; Coote, M. L. *J. Phys. Chem. A* **2010**, *114*, 13442−13444.
(62) Harvey, J. N. *Faraday Discuss.* **2010**, *145*, 487−505.
(63) Mcmullin, C. L.; Jover, J.; Harvey, J. N.; Fey, N. *Dalton Trans.* **2010**, *39*, 10833−10836.
(64) Huang, F.; Lu, G.; Zhao, L.; Li, H.; Wang, Z.-X. *J. Am. Chem. Soc.* **2010**, *132*, 12388−12396.
(65) Cramer, C. J.; Truhlar, D. G. *Acc. Chem. Res.* **2009**, *42*, 439−497.
(66) Sugiyama, A.; Ohnishi, Y.-y.; Nakaoka, M.; Nakao, Y.; Sato, H.; Sakaki, S.; Nakao, Y.; Hiyama, T. *J. Am. Chem. Soc.* **2008**, *130*, 12975−12985.
(67) Liang, Y.; Liu, S.; Xia, Y.; Li, Y.; Yu, Z.-X. *Chem.—Eur. J.* **2008**, *14*, 4361−4373.
(68) Yu, Z.-X.; Houk, K. N. *J. Am. Chem. Soc.* **2003**, *125*, 13825−13830.
(69) Strajbl, M.; Sham, Y. Y.; Villà, J.; Chu, Z. T.; Warshel, A. *J. Phys. Chem. B* **2000**, *104*, 4578−4584.
(70) Mammen, M.; Shakhnovich, E. I.; Deutch, J. M.; Whitesides, G. M. *J. Org. Chem.* **1998**, *63*, 3821−3830.
(71) Hermans, J.; Wang, L. *J. Am. Chem. Soc.* **1997**, *119*, 2707−2714.
(72) Amzel, L. M. *Proteins: Struct., Funct., Bioinf.* **1997**, *28*, 144−149.
(73) Mei, Y.; Averill, D. J.; Allen, M. J. *J. Org. Chem.* **2012**, *77*, 5624−5632.
(74) Mei, Y.; Dissanayake, P.; Allen, M. J. *J. Am. Chem. Soc.* **2010**, *132*, 12388−12873.
(75) Krężel, A.; Lisowski, J. *J. Inorg. Biochem.* **2012**, *107*, 1−5.
(76) Kobayashi, S.; Mori, Y.; Fossey, J. S.; Salter, M. M. *Chem. Rev.* **2011**, *111*, 2626−2704.
(77) Mashiko, T.; Kumagai, N.; Shibasaki, M. *J. Am. Chem. Soc.* **2009**, *131*, 14990−14999.
(78) Aspinall, H. C. *Chem. Rev.* **2002**, *102*, 1807−1850.
(79) Shibasaki, M.; Yoshikawa, N. *Chem. Rev.* **2002**, *102*, 2187−2210.
(80) Inanaga, J.; Furuno, H.; Hayano, T. *Chem. Rev.* **2002**, *102*, 2211−2226.